BNL-101877-2014-TECH
AD/RHIC/RD/94;BNL-101877-2013-IR

Conceptual Design of the RHIC Dump Core

A. J. Stevens

September 1995

Collider Accelerator Department
Brookhaven National Laboratory

U.S. Department of Energy
USDOE Office of Science (SC)

DISCLAIMER

AD/RHIC/RD–94

RHIC PROJECT

Brookhaven National Laboratory

Conceptual Design of the RHIC Dump Core

A. J. Stevens

September 1995

Conceptual Design of the RHIC Internal Dump Core

I. Overview

Conceptually, the internal dump consists of a "core" whose purpose is to absorb the energy of the beam, and surrounding shielding whose purpose is to attenuate radiation. Design of the core for an internal dump has two problems which must be overcome. The first problem is preserving the integrity of the dump core. The bunches must be dispersed laterally an amount sufficient to keep the energy density from cracking the dump core material. Since the dump kickers in RHIC are only ~ 25m upstream of the entrance face of the dump, this is a difficult problem. The second problem, not addressed in this note, is that dumping the beam should not quench downstream magnets. Preliminary calculations related to both of these problems have been presented in earlier notes.[1,2]

A very crude sketch of the dump system is shown in Fig. 1.[3] This figure shows a plan view (on the beam line) of 5 kicker modules deflecting the beam onto the dump. The deflection, as shown, is in the horizontal direction and directed toward the center of the ring.[4] The geometry near the beginning of the dump is somewhat complicated, even conceptually. Fig. 2 shows a sketch of this region. For impedance reasons, the beam pipe must avoid making a large angle with respect to the beam direction. The aborted beam passes through a slot in the "dump window" as shown in this figure. It then enters the "dump core proper", the first segment of which is a block of a material known as Carbon-Carbon (C-C) which is discussed below. At some distance into the dump a "vacuum window" exists which is welded to the beam pipe. The purpose of this window is to isolate the remainder of the dump from the ring vacuum. Note that gasses from the C-C block in front of this window can migrate through the slot into the ring vacuum. It is therefore necessary to pump on the region in front of the vacuum window as indicated very schematically in Fig. 2.

The entrance region described in the preceding paragraph differs from a conventional internal dump which would have a solid dump window, perhaps made of a titanium alloy, through which the deflected beam would pass. However, the short lever arm between the dump kicker magnets and the dump entrance makes bunch dispersion of the Au beam, whose dE/dx is extremely large, very difficult. Although considerable time was devoted to study of possible magnetic deflection systems which would achieve sufficient dispersion to preserve the integrity of a titanium alloy window, such systems — given the lever arm constraint — appear to be difficult (or impossible in certain failure modes) and expensive. The current plan is therefore to preserve the vacuum integrity by pumping rather than attempt to preserve the dump window integrity by varying magnetic deflection.

Fig. 3 shows the displacement on the upstream face of the C-C block (hereafter referred to as the dump face — see Fig. 2) vs. time that the kicker magnets are designed to achieve.[5] There is a nominal gap of 1 μsec in the beam (4 missing bunches out of 57) during which the kicker magnetic field rises. The oscillating and rising field after 1 μsec disperses the bunches. Fig. 4 shows the displacement on the dump face of the centers of about 1/3 of the 53 bunches (at full

energy) to illustrate the dispersion obtained by the kicker function shown in Fig. 3. The maximum bunch density for Au under worst case conditions (full energy and 15π emittance) where the beam sigma in the horizontal direction is 0.0648 cm is equivalent to 9.7 bunches on top of one another.

The purpose of the remainder of this note is to design the layout of the materials which form the dump core. To complete this overview, however, several conceptual sketches are presented of the dump in its entirety.

Fig. 5 shows a cross section of the dump core near its upstream position. The core is shown as a 28 cm. × 28 cm. rectangular region, consisting primarily of steel, but with a carbon region on the side that the beam is dumped. Fig. 6 shows a cross section of the dump on a larger scale. The core is on a movable plate within steel shielding and with marble walls which exist to reduce the induced activity (from the activated steel) to a small level.[6] Fig. 7 shows a plan view of the entire dump. As shown, the steel shielding extends only 3m, whereas the dump core extends the full 5.2m length of the dump. Again, the beginning of the dump is very schematic in nature.

The final remarks in this overview concern the aperture of the dump which is shown (e.g., Fig. 4) to be an ellipse with semi-major axis of 23mm and semi-minor axis of 21mm. This aperture is considerably larger than considered previously.[1,2] The beam center line is displaced 6.5mm so that the edge of the dump is 16.5mm from the beam line. The displacement exists so that an *injection energy* bump could move the beam to the geometrical dump center and thus give greater aperture at this lattice position at injection if desired. The table below shows the aperture limitations of the dump described here. For the case of the displaced center line (no bump) the dump is the limiting fixed horizontal aperture in the machine.

Table 1. Dump Aperture Limitations

	β ($\beta^* = 10$m)	σ (Au,Inj., $\varepsilon = 15\pi$)	Aperture (no bump)	Aperture (bump)
Horizontal	36.2m (Exit)	2.68mm	6.1σ	8.6σ
Vertical	29.0m (Entrance)	2.40mm	8.4σ	8.7σ

II. Materials Properties

The limitation of the (solid) materials in the RHIC dump is set by stress caused by thermal shock. The analysis employed in this note (Section IV below) is based on a single ANSYS calculation which was performed for a titanium alloy.[7] The estimated stresses for other materials are assumed to be related to the calculated material by the corresponding values of:

$$f = \frac{Y \times \alpha \times \Delta T}{T_S}$$

Here Y is the elastic (Young's) modulus, α the coefficient of linear expansion ΔT the maximum temperature rise (in a time interval short in comparison to heat transfer times), and T_S the material tensile strength. This is shown to be true for any *component* of stress in a simple analytic model

developed by Sievers.[8] For non-metals, a corresponding expression exists for the modulus of compression and compressive strength.

The stress evaluation will be fully discussed in Section IV below. The reason for mentioning it here is to point out the properties of materials which must be estimated to evaluate the stress. In principle, the values of Y, α, C_p (specific heat, used in obtaining ΔT), and T_S must be known as a function of temperature, although the temperature dependence for metals is rather small in the temperature range considered here.

(A) *Carbon-Carbon*

C-C is a composite material consisting of carbon fibers in a carbon matrix. It has a measured thermal shock resistance much superior to conventional graphites,[9] but is more expensive. The particular form of C-C described here is called fine weave 2·2·3 Carbon-Carbon whose properties are provided by the manufacturer.[10] The numbers relate to the fiber weave in the composite. The "3 fiber" orientation is defined as the z direction below, and the 2·2 plane as the x direction. However, there is very little directional asymmetry in this form of C-C.

The thermal expansion coefficient is not given directly in Ref [10]. The actual data is thermal strain (δL/L) as a function of temperature. This quantity is essentially zero between room temperature and 1000 °F, after which it rapidly rises (in both orientations). The value of α was estimated by "fitting" (zero constraints) a cubic to data given in Ref [10] between room temperature and 3000 °F, and differentiating the resulting equation to obtain the estimate of α. The equations so obtained are the following:

$$\alpha_z = -1.0150\times10^{-6} + 4.2954\times10^{-9}\,\Delta T - 1.3124\times10^{-12}\,\Delta T^2$$
$$\alpha_x = -.96475\times10^{-6} + 4.0826\times10^{-9}\,\Delta T - 1.1449\times10^{-12}\,\Delta T^2$$

In these expressions (which differ very little) ΔT is the temperature rise relative to room temperature in °C. The value of α_z given by this equation is shown in Fig. 8.

Table 2 below shows the remaining quantities of interest.

Table 2 Mechanical Properties of C-C

Quantity	Units	Value at RT	Value at 1093°C
Tensile Modulus (z)	10^6 psi	14.0	13.2
Tensile Modulus (x)	"	7.94	8.38
Tensile Strength (z)	10^3 psi	49.7	44.7
Tensile Strength (x)	"	26.4	26.7
Compressive Modulus (z)	10^6 psi	12.7	9.47
Compressive Modulus (x)	"	7.28	6.76
Compressive Strength (z)	10^3 psi	24.1	28.0
Compressive Strength (x)	"	14.2	17.6

The directional differences are negligible in comparison to the quoted errors on these quantities which is typically of order 10%. Assuming a linear T dependence, Fig. 9 shows the quantity of interest, f, in the x direction for both tension and compression as a function of temperature. This figure will be referred to in Section IV below.

Another quantity which has a strong (and beneficial in this case) temperature dependence is the specific heat. Fig. 10 shows a formula for C_p in ATJ graphite derived from data given elsewhere.[11] It is assumed that the specific heat for C-C is the same as graphite.

(B) *Steel* (Stainless Type 17-7PH)

As discussed in the preceding section, after some length of C-C, a vacuum window is present which isolates the remainder of the dump from the ring vacuum. For ease in construction and maximum reliability the window will be made of a high-strength stainless steel. The mechanical properties of type 17-7PH[12,13] are shown in Table 3 below.

Temperature (°C)	Modulus (10^6 psi)	Tensile Strength (10^3 psi)
20	29.0	185
205	25.9	—
427	—	143

The value of α for 17-7PH is given by:[14]

$$\alpha = 4.749 \times 10^{-6} + 2.362 \times 10^{-8}\, T - 6.123 \times 10^{-12}\, T^2$$

with T in degrees Kelvin. The specific heat will be taken to be 0.085 Cal/g°C,[15] independent of temperature.

(C) *Graphite*

A region of graphite follows the steel window for some distance before transition to solid steel is possible. A *thin* window of steel (thin compared to a radiation length) has less energy density than a thick section because no build-up of the electromagnetic cascade occurs in a thin window. This is the reason a graphite section is required between the steel window and the section of the dump core which is solid steel.

It will be shown below that the satisfying the stress requirements on the steel window leads to a very modest value for the temperature rise ΔT in the graphite. For that reason, only room temperature properties for graphite are needed. The room temperature properties for Grade G20[17] graphite are given in Table 4 below.

Table 4 G20 Graphite Properties

Property	With Grain	Against Grain
Tensile Modulus (10^6 psi)	1.34	1.31
Compressive Modulus (10^6 psi)	1.16	1.10
Tensile Strength (10^3 psi)	4.00	3.90
Compressive Strength (10^3 psi)	13.0	9.50
Coeff. Thermal Exp.* (10^{-6} cm/cm °C)	3.2	3.8

* Rm. Temp to 600 °C

III. Energy Deposition Calculations

Energy Deposition calculations were done with the CASIM Monte Carlo program.[17] Each incident primary was sampled from a distribution of 53 bunches whose transverse position on the dump face had been calculated from a separate program which simulated the rise of the abort kicker magnetic field shown in Fig. 3. For convenience, the beam divergence was ignored. The transverse size of each bunch was appropriate for an Au beam at full energy and 15π mm-mrd emittance.[18]

The energy deposition density in C-C is shown in Fig. 11. The ordinate in this figure for the circles shown is GeV per cm^3 per Au ion. For comparison, the "+" marks in this figure show energy density for 250 GeV protons. In this case the ordinate is GeV per cm per 100 protons. Since there are 100 more protons than Au ions at design intensity this normalization directly compares the effects of the two different beams. As shown, the Au dominates the energy density until a depth of ~ 55 cm. This is due, of course, to the large dE/dx and short interaction length of the Au ions.

As mentioned in the preceding section, when a steel region is thick in comparison to the radiation length an electromagnetic build up occurs. Fig. 12 shows the results of 2 additional CASIM calculations. In the first calculation, indicated by "+" symbols in Fig. 12, a transition from carbon[21] to steel was assumed to occur at 150 cm. from the dump face and in the second (indicated by open circles) at 250 cm. These calculations were done for 250 GeV/c protons. The ordinate is again in energy density per 100 protons simply to illustrate (with Fig. 11) the relative energy deposition as a function of both depth and particle species.

IV. Stress Limits

As mentioned in Section II above, Sievers[8] has demonstrated, in the context of a simple model for beam heating, that thermal stresses are proportional to the product $Y \times \alpha \times \Delta T$. This also follows from units analysis. What *multiplies* this expression can be almost arbitrarily complex. In Sievers model, simple constant multipliers exist for "quasi-static" stress and an infinite Bessel function series describes the time dependent shock stress enhancements due to very rapid temperature increases.

We rely here on an ANSYS transient calculation[7] performed for a situation very similar to that which exists here. The calculation was made at a time when an attempt was being made to disperse the bunches with a magnetic sweeper as well as a kicker, and was directed toward estimating the thermal stresses in a thin Ti alloy dump window. Eight bunches, with 10 nsec. width and 220 nsec. spacing were incident on the window. The lateral spacing of the bunches was such as to produce a bunch overlap of 3.9, i.e., the "hot-spot" was equivalent to 3.9 bunches on top of one another.

The result of the calculation was a maximum stress (in time) of 124,000 psi. **This is 2.3 times the $Y\times\alpha\times\Delta T$ value** where Y and α were the assumed (constant with temperature) values for the alloy considered and ΔT is the hot-spot temperature. This value is a relatively small shock enhancement when compared to those found in the simple model of Sievers. This follows from the fact that the stress waves caused by each bunch are out of phase with waves from other bunches. The identical situation is encountered in the current design. As mentioned in the introduction, the kicker rise shown in Fig. 3 produces a hot-spot equivalent to 9.7 overlapped bunches. This comes from 13 bunches of the 53 simulated.[20]

The algorithm for stress evaluation is therefore to multiply $Y\times\alpha\times\Delta T$ by 2.3 and say that this quantity should be less than some fraction of the tensile strength (or compressive strength if relevant). A limit of 1/3 of the strength is a conservative number which allows for both failures in some of the kicker modules and errors in materials parameters. In this case:

$$2.3\times Y\times\alpha\times\Delta T<\frac{T_s}{3} \text{ or}$$

$$f=\frac{Y\times\alpha\times\Delta T}{T_s}<0.145$$

The evaluation of f as a function of position now follows. For historical reasons we consider the design intensity to be 57×10^9 Au ions (or 57×10^{11} protons). This corresponds to no missing bunches during the abort kicker risetime. In practice, the gap in the beam will be made as small as possible to maximize the collider luminosity.

(A) *Entrance Energy Deposition*

For C-C, the criteria adopted above is far too conservative. In the test described in Ref [10] no fractures were observed under conditions so severe that the C-C began to sublime at 2000 °C. The entrance energy deposition density is shown in Fig. 11. At the beginning of the dump, the 1.1×10^2 GeV/cc at design intensity gives 135 Cal/g. Using the specific heat shown in Fig. 10 gives ΔT = 480 °C. The stress limit calculated in Ref [8] is the "equivalent stress" whose direction is not obvious. Using the mid point of the two curves shown in Fig. 9 gives $f = 0.13$. Since this is even within the adopted criteria, **the entrance deposition density has a very large margin of safety**.

(B) *Steel Vacuum Window*

The vacuum window determines the length of the C-C section. For a *thin* window the energy density in steel at some depth is obtained from the energy density in carbon shown in Fig. 11 by simply scaling by dE/dx, i.e.,

$$\frac{\Delta E}{\Delta V}(in\,Energy/g) = constant \times \frac{dE}{dx}(in\,Energy/g/cm^2)$$

To obtain the energy density in a thin section of steel at some point in Fig. 11 one multiplies the value shown in Fig. 11 by the ratio of the density times the minimum dE/dx values. This turns out to be 3.6. Here we simply invert this process. A curve similar to Fig. 9 is readily obtained for the 17-7PH steel from the materials properties in the preceding section. The *f* value of 0.145 gives an allowable (with safety margin of course) ΔT in steel of 76 °C. This gives an energy density of 6.45 Cal/g. Working backwards, an energy density per Au ion of 22.5 GeV per cc in steel or 6.25 GeV/cc in carbon. From Fig. 11 this occurs at 43.5 cm or 17 inches. **A length of 17 inches of CC is therefore required before the vacuum window assuming it is made of 17-7PH steel.**

(C) *Transition to Graphite*

Immediately behind the steel vacuum window is a region of graphite. The energy density of 6.25 GeV/cc in carbon is a ΔT of only 43 °C. The value of *f* for the worst case in Table 4 (tension, against the grain) is only 0.055. Given the steel window, graphite is a non problem as one would expect.

(D) *Bulk Steel Transition*

The transition to bulk steel is obtained from Fig. 12. As noted in (B) above, the f = 0.145 criteria translates to an energy density of 22.5 in the ordinate of this figure. The transition at Z = 150 cm. does not meet this criteria whereas the transition at 250 cm is 12, *a factor of 1.9 more safe than required.* One can either make the transition to steel earlier or use a steel whose material properties are considerably worse than 17-7PH. The latter course will likely be adopted although the form of bulk steel has not yet been determined.

V. Summary

In summary, the design of the dump core as currently envisaged consists of the following materials. (1) 43.5 cm. or more of a thermal shock resistant material known as Carbon-Carbon (C-C), (2) a steel vacuum window which isolates the remainder of the dump from the ring vacuum, (3) a region of ordinary graphite which extends to 2.5 meters from the beginning of the C-C, and (4) bulk steel which extends the remainder of the total core length of 5.2m. At RHIC design intensity, analysis indicates that such a dump core has a considerable safety margin for thermal stress which includes the shock associated the very rapid (~ 10 nsec.) temperature rises

created by a beam bunch. The price paid for the stress resistance is that the C-C section is exposed to the ring vacuum which necessitates pumping on this part of the dump to reduce out-gassing to a tolerable level.

References/Footnotes

1. A. J. Stevens, "Maximum Energy Deposition Densities in the Internal Dump," AD/RHIC/RD-41, June, 1992.

2. A.J. Stevens, "Preliminary Study of Energy Deposition Downstream of the Internal Dump," AD/RHIC/RD-33, January, 1992.

3. The relative positions and lengths along the beam line (Z coordinate) in Fig. 1 are meant to be reasonably accurate. Z = 0 marks the valve at the cold to warm transition following Q3 in the outer arc at 10 o'clock. In this system the center of the kicker string is at Z = 4.2m which is about 25m from the "face" of the dump. The dump is 5.2m in length. The distance between the downstream of the dump and the beginning of the Q4 cold mass (Q4T) is about 2m.

4. The fact that the sense of direction of the aborted beam is toward ring center is important, but is not relevant to the purpose of this note.

5. C. Pappas, private communication.

6. A. J. Stevens, "Radiation Environment and Induced Activity Near the RHIC Internal Dump," AD/RHIC/RD-48, November, 1992. See also memorandum to T. Robinson from A.J. Stevens on the subject "Estimate of Dose Rate Close to the C-C Dump Core from Induced Activity" dated 08/14/95.

7. N. Tsoupas, A.J. Stevens, E.S. Rodger, "Calculation of Stresses Induced by RHIC Beam on a Titanium Foil," AD/RHIC/RD-33, September, 1995.

8. P. Sievers, "Elastic Stress Waves in Matter Due to Rapid Heating by an Intense High-Energy Particle Beam," CERN LABII/BT/74-2, June, 1974.

9. C.D. Croessmann, et. al., "Thermal Shock Testing of Candidate Compact Ignition Tokamak Graphites," Fusion Technology, Vol 15, pp. 127-135, January 1989.

10. "Mechanical and Thermal Properties of Fine Weave 2·2·3 Carbon-Carbon," Prepared by: Fiber Materials, Inc., FMI-PmO-94-0235, November 1994. [The density is 1.77 g/cc].

11. Y.S. Touloukian et. al. Eds., "Thermophysical Properties of Matter," IFI/Plenum, New York, Vol. 5, pp. 9-13, 1970.

12. "Materials Engineering," Vol. 82 No.4, Reinhold Publishing Co. Inc., 1975. This Reference is for properties in Table 3 at 20 °C and 427 °C [800 F].

13. "Metals Handbook," Ninth Edition, Vol. 3, p. 203, American Society for Metals, Metals Park, Ohio, 1980. The modulus value in Table 3 at 205 °C is for stainless type AM-355. This is in the same class of steels as 17-7PH (precipitation-hardening stainless steels) with similar composition (~ 16% Cr and 5% Ni).

14. Y.S. Touloukian et. al., Vol. 12, p. 1138.

15. Ibid., Vol. 4, p. 698.

16. Grade G20 material properties supplied by the manufacturer, Graphite Engineering & Sales Co., Greenville MI.

17. A. Van Ginneken, "CASIM. Program to Simulate Hadronic Cascades in Bulk Matter," Fermilab FN-272, 1975. The modification of CASIM for heavy ions is described in Ref [1].

18. The beam size was taken to be the same for incident protons which translates to an emittance of ~35π.

19. No distinction between graphite and C-C is made in the CASIM calculations. Both are assumed to have a density of 1.77 g/cc.

20. The meaning of this statement is that 13 bunches are within 2.5σ of the hotspot. This was also the criteria for the 8 bunches considered in Ref. [8].

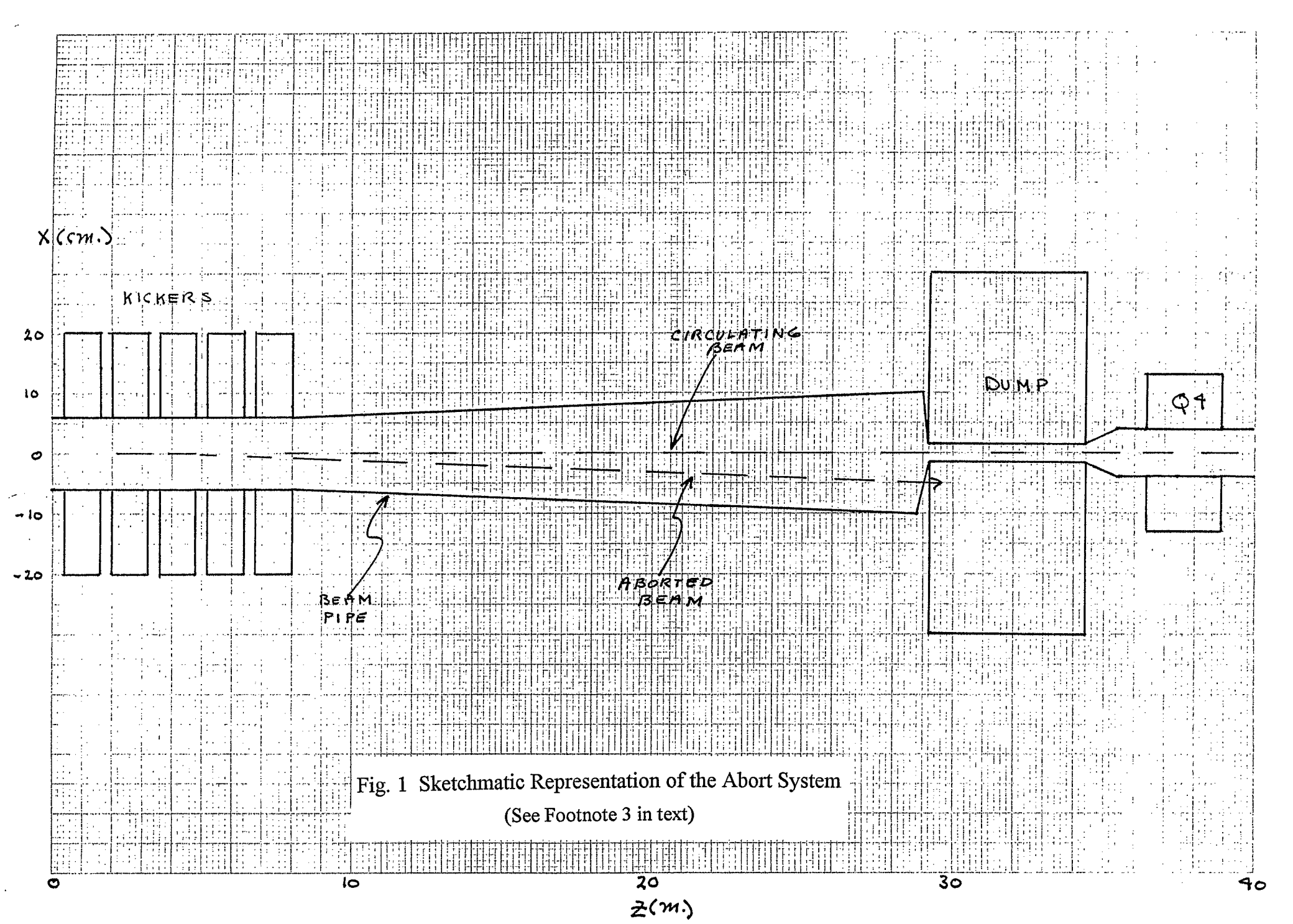

Fig. 1 Sketchmatic Representation of the Abort System

(See Footnote 3 in text)

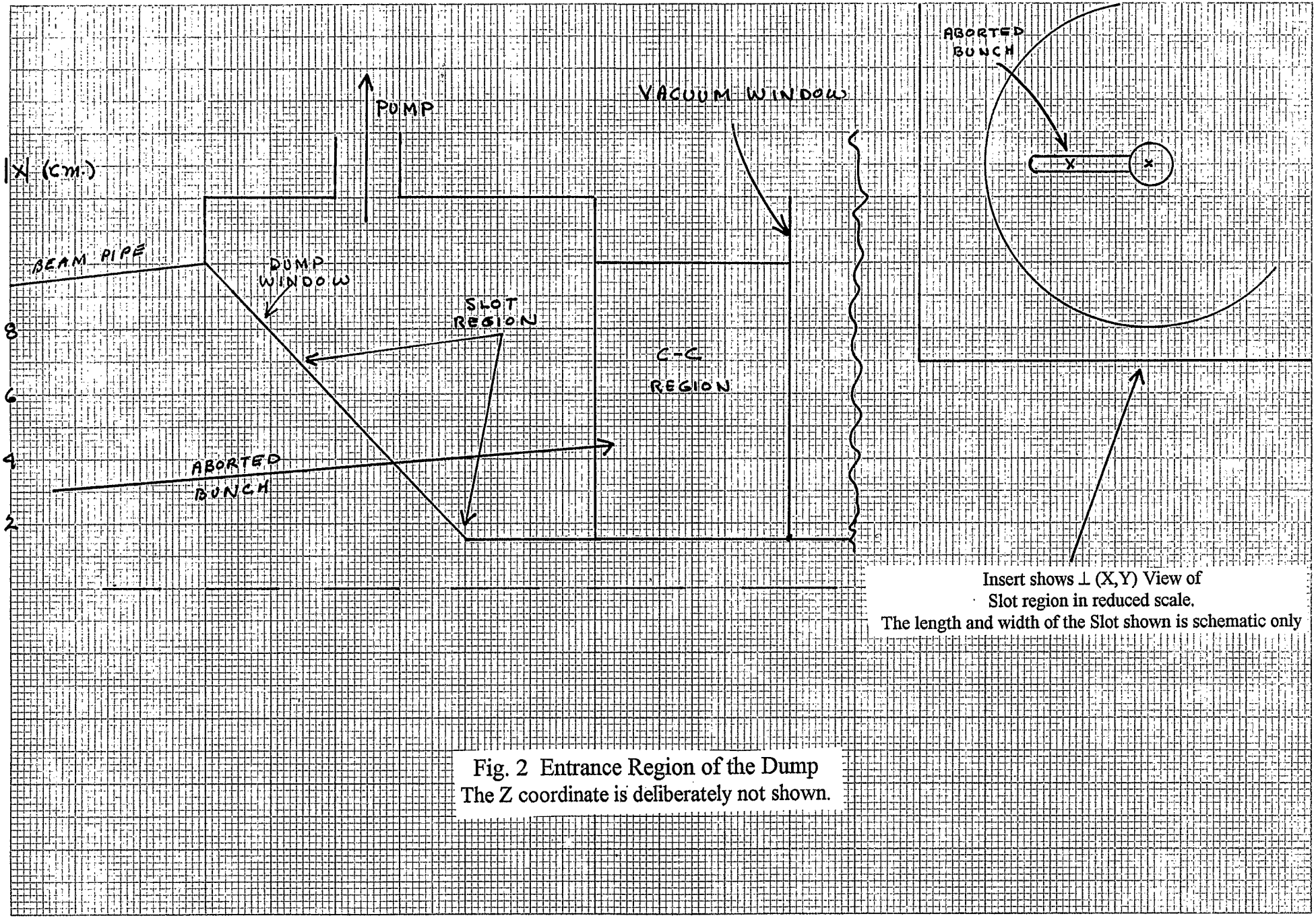

Fig. 2 Entrance Region of the Dump
The Z coordinate is deliberately not shown.

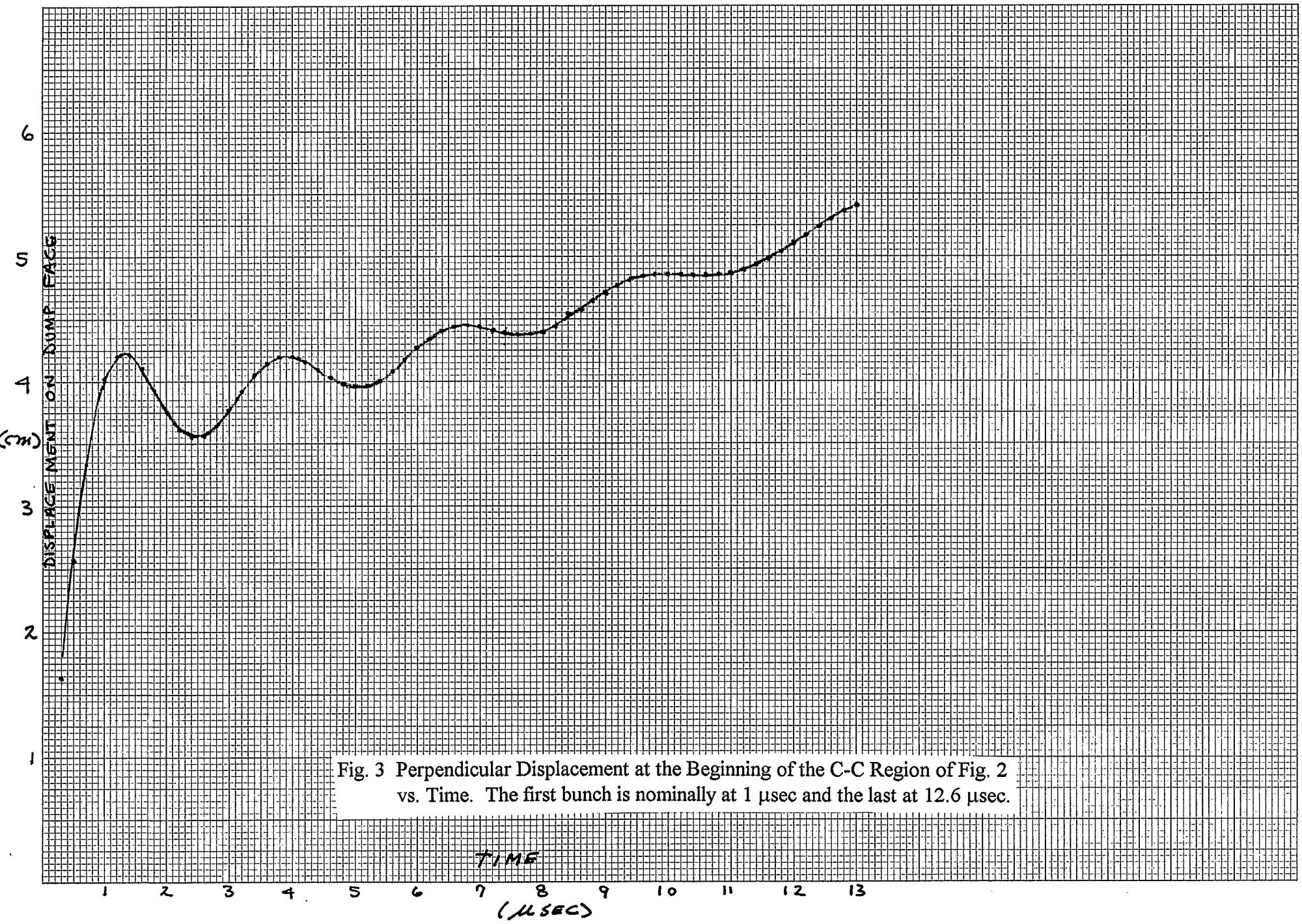

Fig. 3 Perpendicular Displacement at the Beginning of the C-C Region of Fig. 2 vs. Time. The first bunch is nominally at 1 μsec and the last at 12.6 μsec.

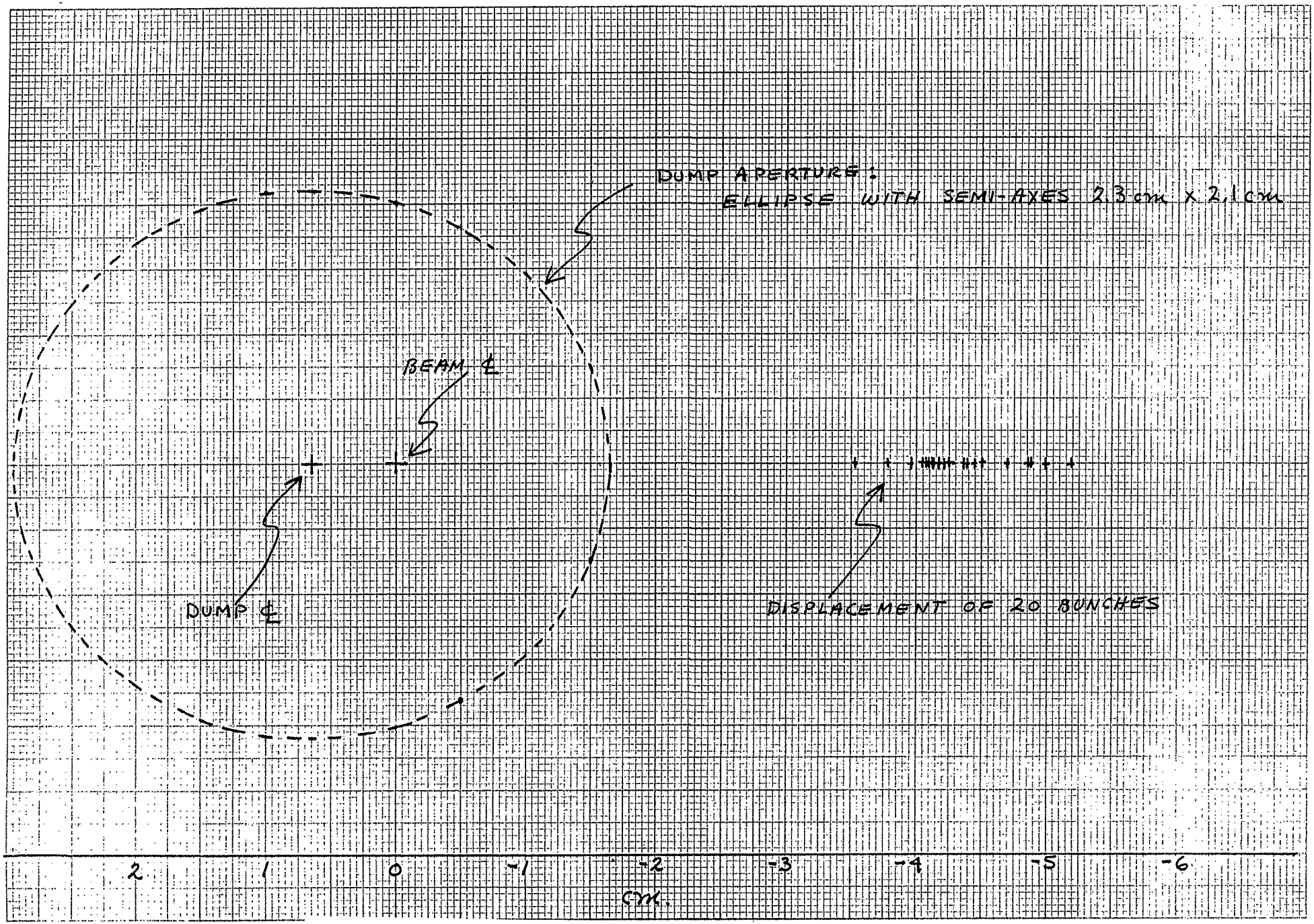

Fig. 4 Transverse Displacement of 20 Bunches Illustrating Dispersion Achieved by the Kicker Function Shown in Fig. 3

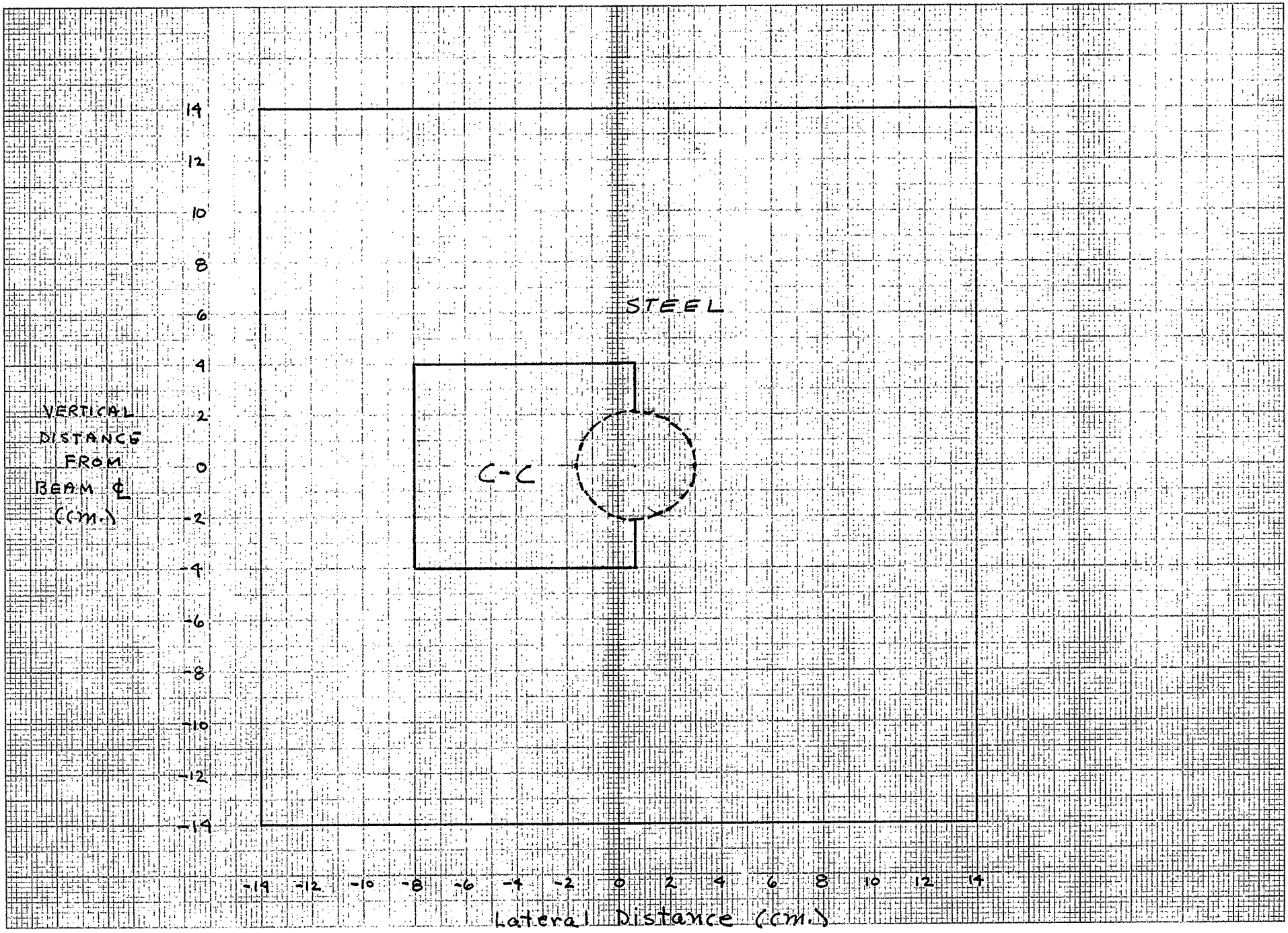

Fig. 5 Cross Section of the Dump Core Near the Upstream End

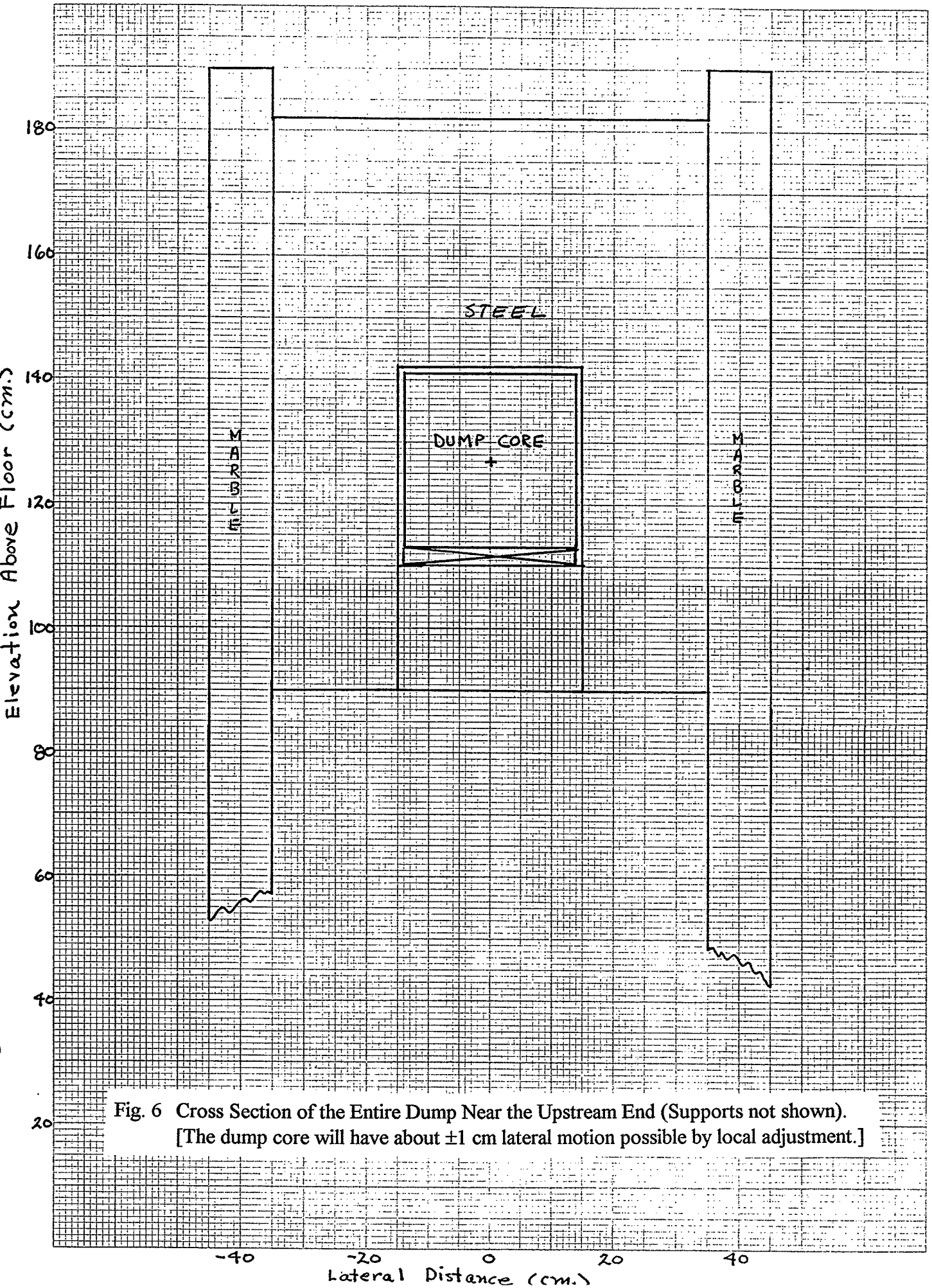

Fig. 6 Cross Section of the Entire Dump Near the Upstream End (Supports not shown). [The dump core will have about ±1 cm lateral motion possible by local adjustment.]

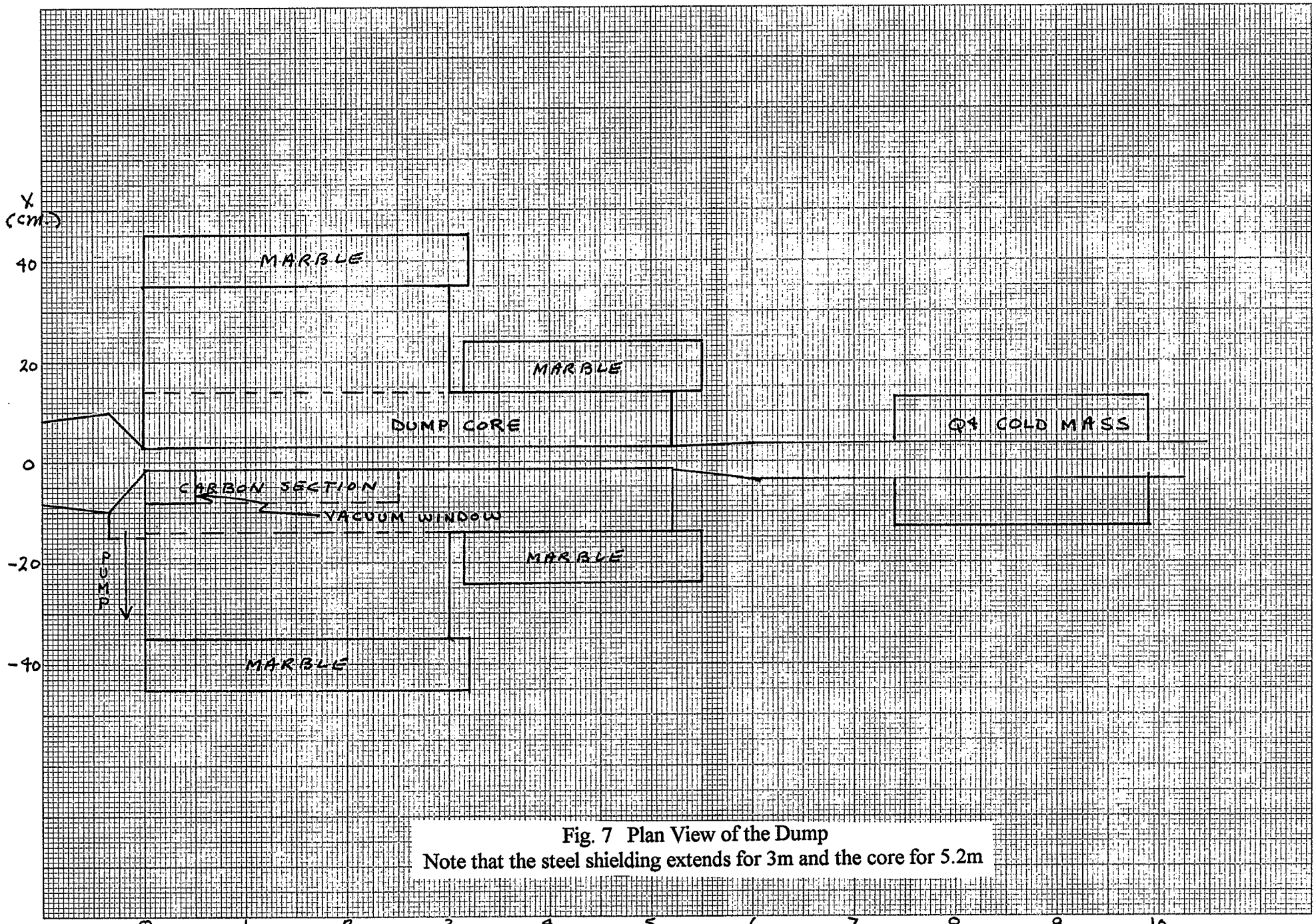

Fig. 7 Plan View of the Dump
Note that the steel shielding extends for 3m and the core for 5.2m

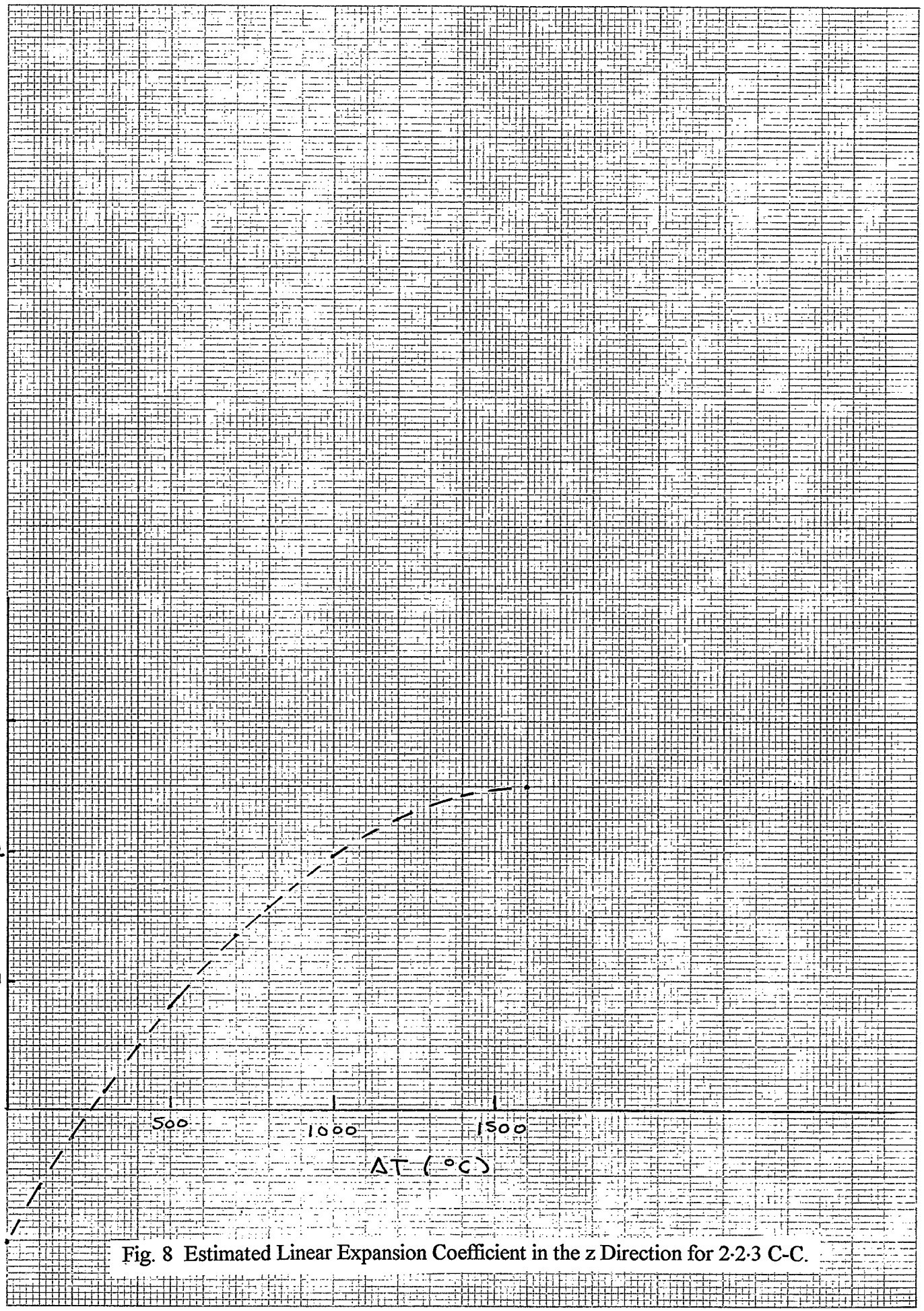

Fig. 8 Estimated Linear Expansion Coefficient in the z Direction for 2-2-3 C-C.

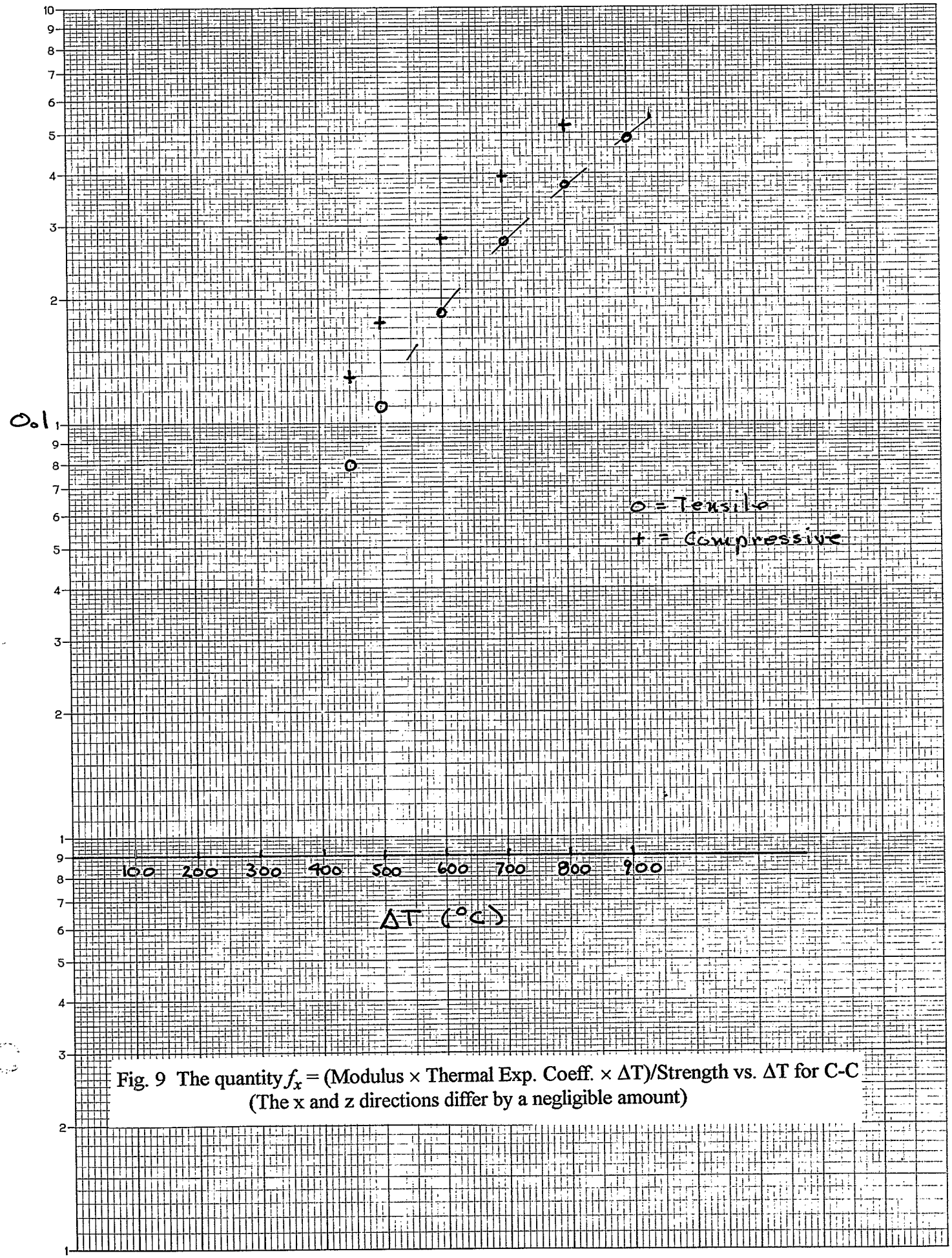

Fig. 9 The quantity f_x = (Modulus × Thermal Exp. Coeff. × ΔT)/Strength vs. ΔT for C-C
(The x and z directions differ by a negligible amount)

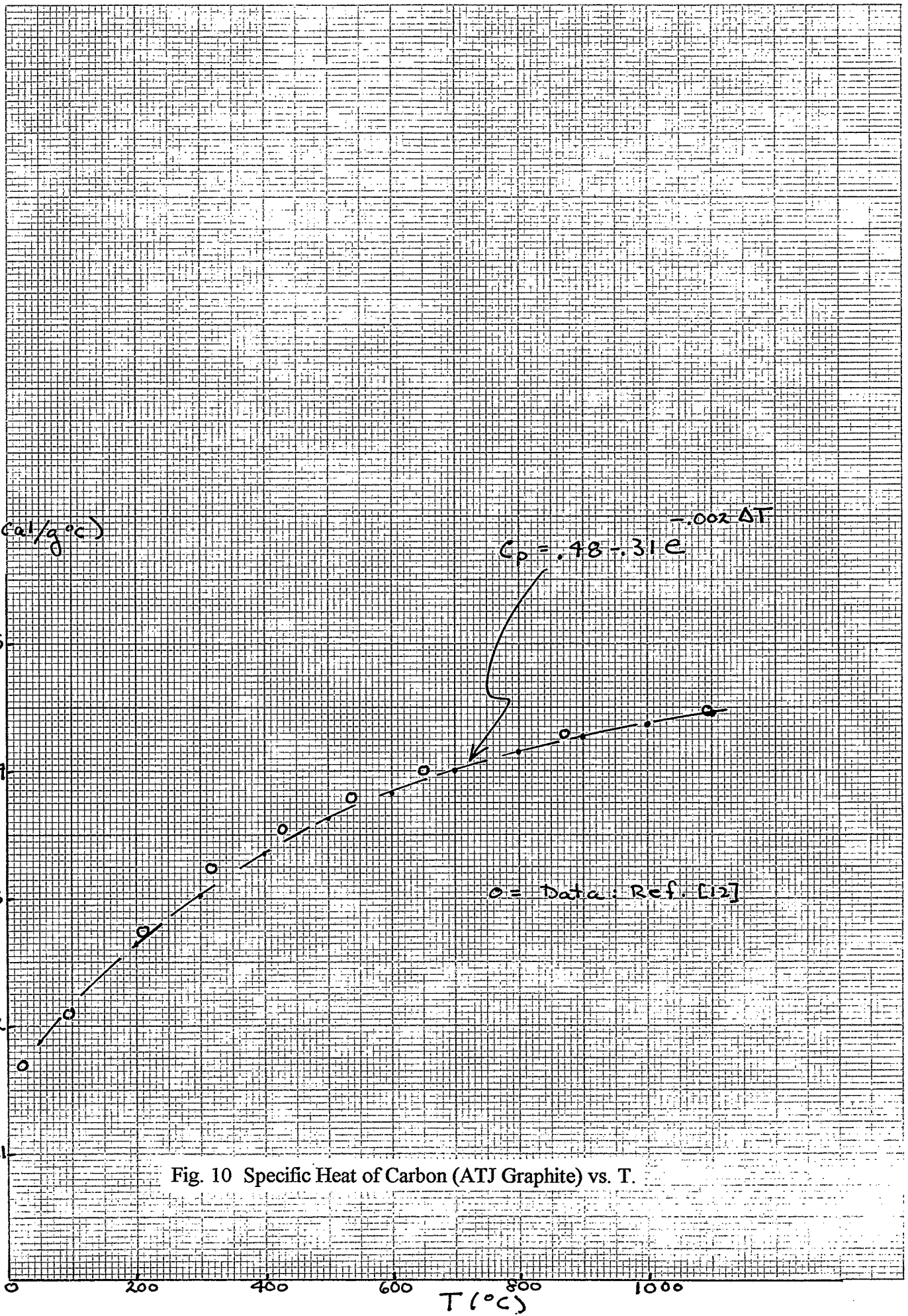

Fig. 10 Specific Heat of Carbon (ATJ Graphite) vs. T.

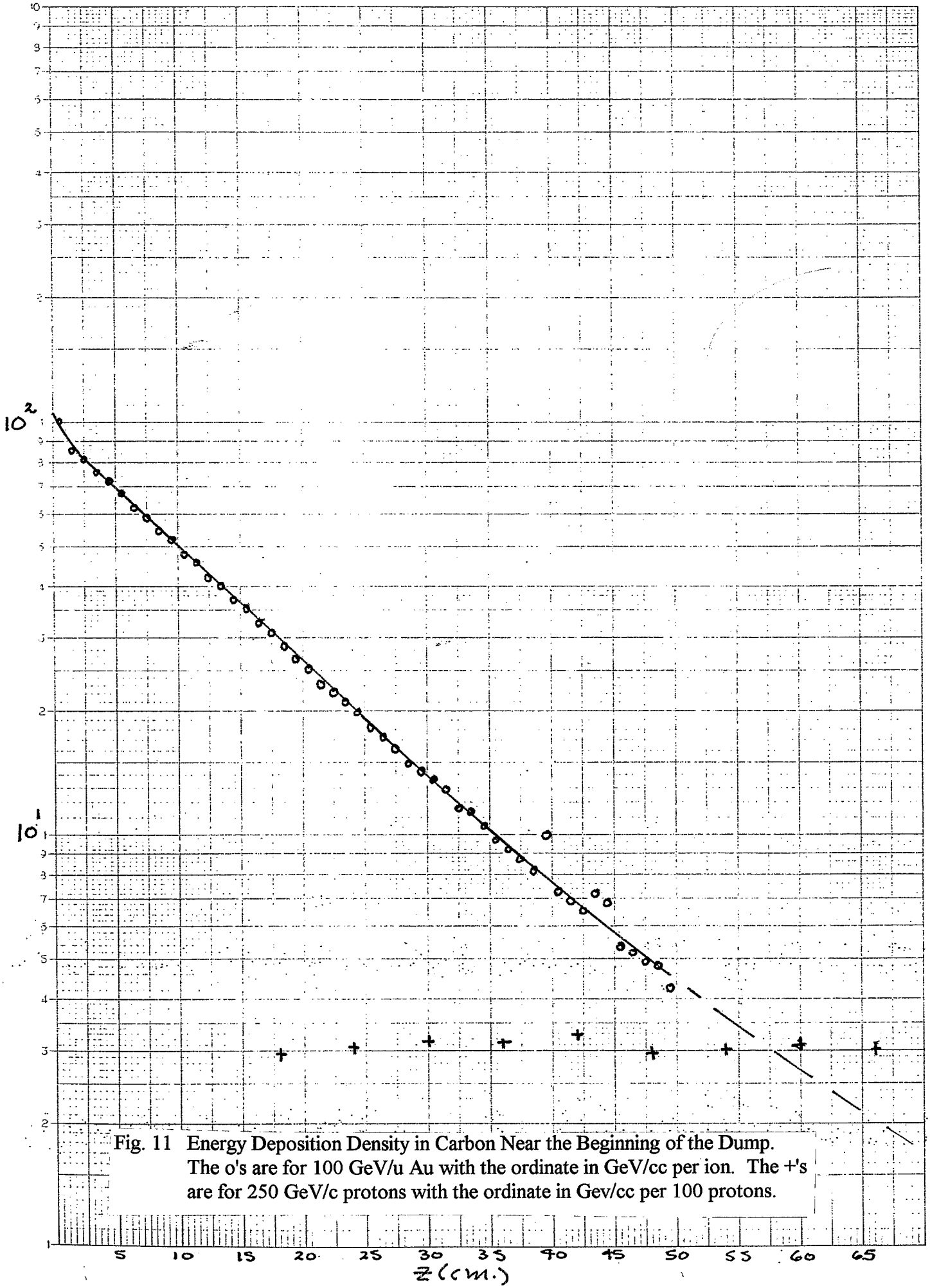

Fig. 11 Energy Deposition Density in Carbon Near the Beginning of the Dump. The o's are for 100 GeV/u Au with the ordinate in GeV/cc per ion. The +'s are for 250 GeV/c protons with the ordinate in Gev/cc per 100 protons.

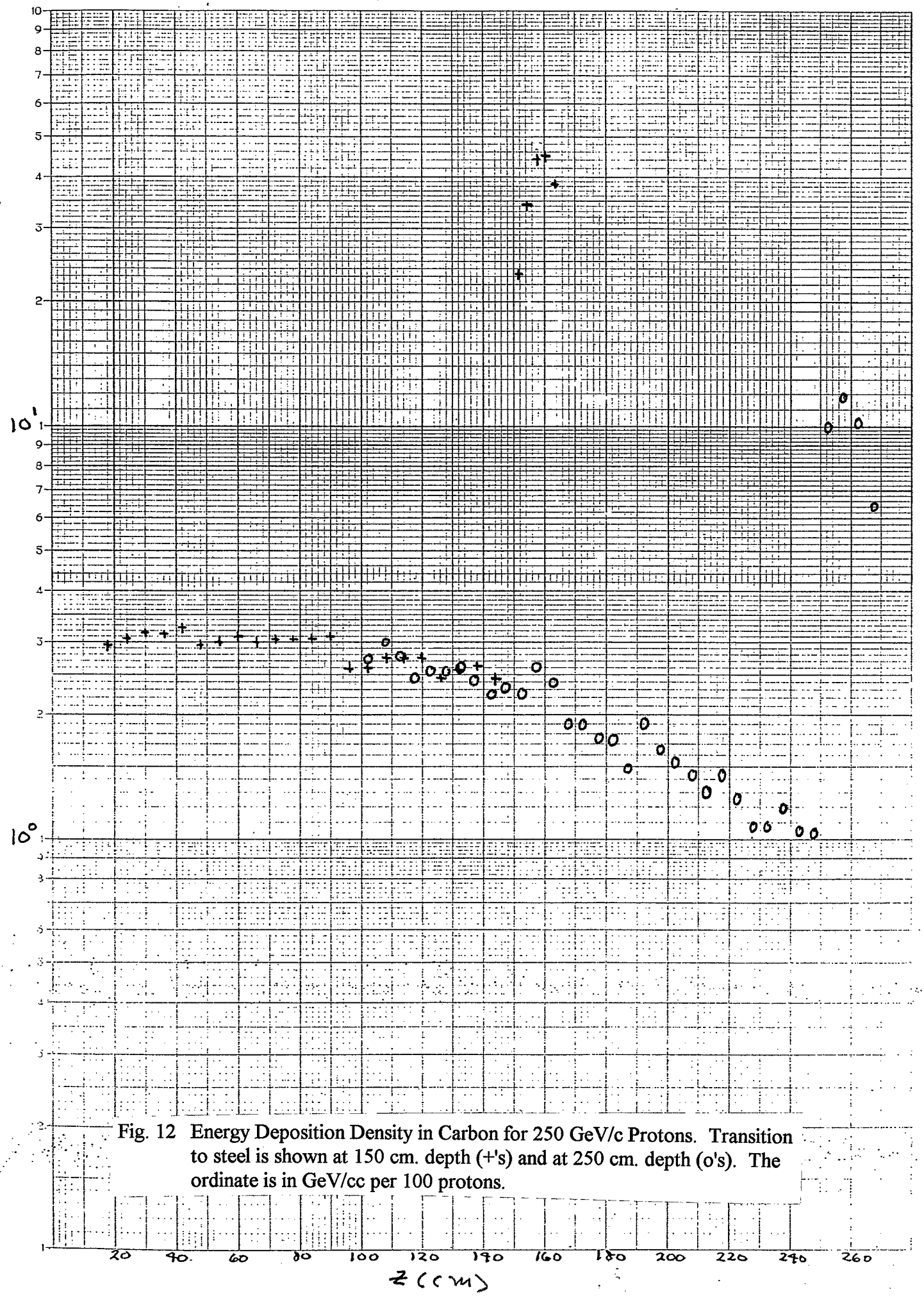

Fig. 12 Energy Deposition Density in Carbon for 250 GeV/c Protons. Transition to steel is shown at 150 cm. depth (+'s) and at 250 cm. depth (o's). The ordinate is in GeV/cc per 100 protons.